ELSEVIER

Fluid Dynamics Research 34 (2004) 1–19

FLUID DYNAMICS RESEARCH

Some fluid-mechanical problems in geophysics—waves in the atmosphere and fault lubrication☆

Hiroo Kanamori

Seismological Laboratory, California Institute of Technology, Pasadena, CA 91125, USA

Received 6 January 2003; received in revised form 26 August 2003; accepted 30 August 2003
Communicated by A. Sasoh

Abstract

Many geophysical processes occurring in the ocean and atmosphere are commonly investigated using fluid mechanics. Tsunami in the ocean, and atmospheric waves excited by volcanic eruptions and other causes are among the most typical problems in geophysics where fluid mechanics plays an important role. Several examples which pertain to the processes in the atmosphere and to earthquake faulting where fluid mechanics plays a key role are discussed in this short review.

Keywords: Acoustic wave; Internal gravity wave; Lubrication

1. Introduction

Fluid mechanics is extensively used in Earth sciences for problems with a long time scale such as convection in Earth's mantle and core. Also, many geophysical processes occurring in the ocean and atmosphere are commonly investigated using fluid mechanics. Tsunami in the ocean, and atmospheric waves excited by volcanic eruptions and other causes are among the most typical problems in geophysics where fluid mechanics plays an important role. The convection problem is extensively discussed in many text books (e.g., Schubert et al., 2001), and is not discussed here. This paper illustrates a few examples from the works in which I was personally involved. These examples pertain to the processes in the atmosphere and to earthquake faulting where fluid mechanics plays a key role.

☆ This paper is a summary of the presentation given at the 2002 Annual Conference of Japan Society of Fluid Mechanics held in Sendai, Japan.

E-mail address: hiroo@gps.caltech.edu (H. Kanamori).

0169-5983/$30.00
doi:10.1016/j.fluiddyn.2003.08.006

2. Excitation of atmospheric waves by volcanic eruptions

The thermal energy emitted by a volcanic eruption excites atmospheric waves and oscillations (Fig. 1). A comprehensive review on this subject is found in Blanc (1985). The most notable is the air wave excited by the 1883 Krakatoa eruption in Indonesia (Harkrider and Press, 1967), and the most recent is that excited by the 1991 Pinatubo eruption in the Philippines. In general, three types of waves can be excited as illustrated by Fig. 1b which shows the dispersion relation for acoustic-gravity waves for an isothermal atmosphere on the frequency-wave number space (e.g., Gill, 1982; Hines, 1960). We summarize the basic concept in the following, taken mainly from Houghton (1986).

2.1. Basic equations and dispersion relation

We take a Cartesian co-ordinate system (x, y, z), with the z-axis taken upward vertical in an isothermal atmosphere, and write the x, y, and z components of the velocity field measured from the stationary state by u, v, and w, respectively. The pressure and density are written as $p + p_0$, and $\rho + \rho_0$ where p_0 and ρ_0 represent the background states and p and ρ, the perturbations from them. Then the equations of state and hydrostatic equilibrium are given by

$$p_0 = \rho_0 R T_0, \qquad \frac{\partial p_0}{\partial z} = -g\rho_0, \tag{1}$$

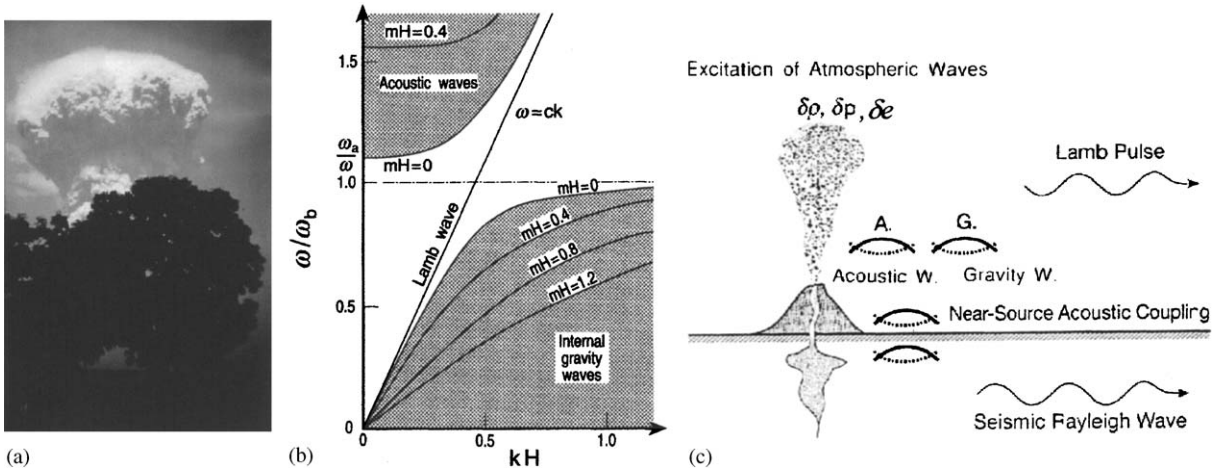

Fig. 1. (a) An eruption of Mount Pinatubo (Courtesy of Dr. J. Mori). (b) Dispersion relation of acoustic-gravity waves in an isothermal atmosphere (modified from Gill (1982)). The vertical axis is the angular frequency, ω, and k and m are the horizontal and vertical wave numbers, respectively, and H is the vertical scale height. (c) Schematic diagram showing the excitation mechanism of atmospheric oscillations by a volcanic eruption. The eruption can be modeled as injection of mass, $\delta\rho$, injection of energy, δe, and perturbation of pressure δp. The thermal energy emitted by an eruption excites acoustic and gravity modes of atmospheric oscillations. The energy of the atmospheric acoustic mode is coupled to the ground and excites seismic Rayleigh waves.

where R is the gas constant of the air. Then p_0 and ρ_0 are given by

$$p_0(z) = p_0(0)\exp[-gz/RT_0] \tag{2}$$

and

$$\rho_0(z) = \rho_0(0)\exp[-gz/RT_0]. \tag{3}$$

In an isothermal atmosphere, the sound velocity c and the scale height H are independent of z and are given by

$$c^2 = \gamma p_0/\rho_0 = \gamma RT_0 \tag{4}$$

and

$$H = RT_0/g, \tag{5}$$

where γ is the specific heat ratio.

The linearized equations for conservation of momentum, conservation of mass, and conservation of energy are given by

$$\rho_0 \frac{\partial u}{\partial t} = -\frac{\partial p}{\partial x},\ \rho_0 \frac{\partial v}{\partial t} = -\frac{\partial p}{\partial y},\ \rho_0 \frac{\partial w}{\partial t} = -\frac{\partial p}{\partial z} - \rho g, \tag{6}$$

$$\frac{\partial \rho}{\partial t} + w\frac{\partial \rho_0}{\partial z} + \rho_0\left(\frac{\partial u}{\partial x} + \frac{\partial v}{\partial y} + \frac{\partial w}{\partial z}\right) = 0 \tag{7}$$

and

$$\frac{\partial p}{\partial t} - g\rho_0 w = c^2\left(\frac{\partial \rho}{\partial t} + w\frac{\partial \rho_0}{\partial z}\right), \tag{8}$$

respectively.

For a plane wave propagating on the x–z plane, assuming the dependence of u, w, p and ρ on x, z, and t in the form

$$\exp(\alpha z)\exp[\mathrm{i}(\omega t + kx + mz)] \tag{9}$$

and substituting it in the linearized equations, we obtain

$$\alpha = 1/2H, \tag{10}$$

and a physical dispersion relation

$$m^2 = k^2\left(\frac{\omega_\mathrm{b}^2}{\omega^2} - 1\right) + \frac{(\omega^2 - \omega_\mathrm{a}^2)}{c^2}, \tag{11}$$

where

$$\omega_\mathrm{b}^2 = \frac{(\gamma - 1)g}{\gamma H} \tag{12}$$

and

$$\omega_\mathrm{a}^2 = \frac{\gamma g}{4H} = \left(\frac{c}{2H}\right)^2. \tag{13}$$

The angular frequency ω_a is called the acoustic cut-off frequency and ω_b is called the Brunt-Väisälä frequency, which is often written as N, too.

The dispersion relation (11) is shown in Fig. 1b. If $c=300$ m/s, then $H=6.6$ km, $\omega_a=0.0229$ s^{-1}, and $\omega_b=0.0207$ s^{-1}. The periods corresponding to ω_a and ω_b are 275 and 304 s, respectively.

2.2. Waves in the atmosphere

Waves are possible only in the stippled regions where the vertical wave number m is real in the dispersion relation given by (11), and on the straight line labeled as Lamb wave. The most common is the Lamb pulse which propagates along the Earth's surface (Figs. 1b and c). The pressure perturbation is limited to the region near the Earth's surface, and the propagation speed is approximately 300 m/s, close to the sound speed. The Lamb pulse has been observed for many large eruptions such as the 1980 Mount St. Helens eruption (Bolt and Tanimoto, 1981). The other two are the atmospheric acoustic (short period) and gravity (long period) waves (Figs. 1b and c). However, they are not commonly observed, partly because of the lack of global networks of pressure sensors (e.g., micro-barographs).

During the large eruption of Mount Pinatubo in the Philippines in 1991, unusual harmonic oscillations with a period of about 230 s and with a duration of a few hours were recorded by seismographs at many stations in the world (Fig. 2) (Kanamori and Mori, 1992; Widmer and Zürn, 1992). Such harmonic waves had not been recognized before, and their cause was not understood immediately. The frequency spectrum of this oscillation exhibits a distinct peak at 0.0044 Hz (228 s), and another, smaller, peak at 0.0037 Hz (270 s) (Fig. 3). The subsequent investigations (Kanamori and Mori, 1992; Kanamori et al., 1994) demonstrated that the atmospheric acoustic oscillations set off by the eruption in the Earth's atmosphere (i.e., waves in the upper-left stippled region in Fig. 1b, where the angular frequency, ω, is higher than the acoustic cut-off frequency, ω_a, given by (13)) excited seismic Rayleigh waves (surface waves) at points near the volcano which were observed worldwide with seismographs, rather than barographs. This situation is illustrated in Fig. 1c.

What follows is a brief description of the method used in Kanamori et al. (1994). Although the temperature in Earth's atmosphere has a vertical variation, we use a simple isothermal atmosphere for a basic understanding of the excitation problems of atmospheric waves. Although the isothermal atmosphere is simple, its density stratification caused by gravity provides the key mechanism for excitation and propagation of acoustic waves and internal gravity waves; it is amenable to analytical approach and is useful for understanding how the two characteristic frequencies, ω_a and ω_b, control the near-source oscillations. In the lower part of Earth's atmosphere, the temperature gradient, about 6.5 K km^{-1}, is smaller than the adiabatic lapse rate, about 10 K km^{-1}, and the difference provides buoyancy necessary for generation of internal gravity waves. The characteristic frequencies are not exactly the same between the isothermal model and Earth's atmosphere, but they are close enough for purposes of the present discussion.

2.3. Excitation of plane waves

When $k=0$, and $\omega>\omega_a$, m in (11) is real, and (9) represents a vertically propagating wave. If $\omega_a>\omega>0$, m is a pure imaginary and (9) represents a vertical oscillation. This result agrees with that of Lamb (1932) who solved the problem in a different way. Following Lamb (1932), we can

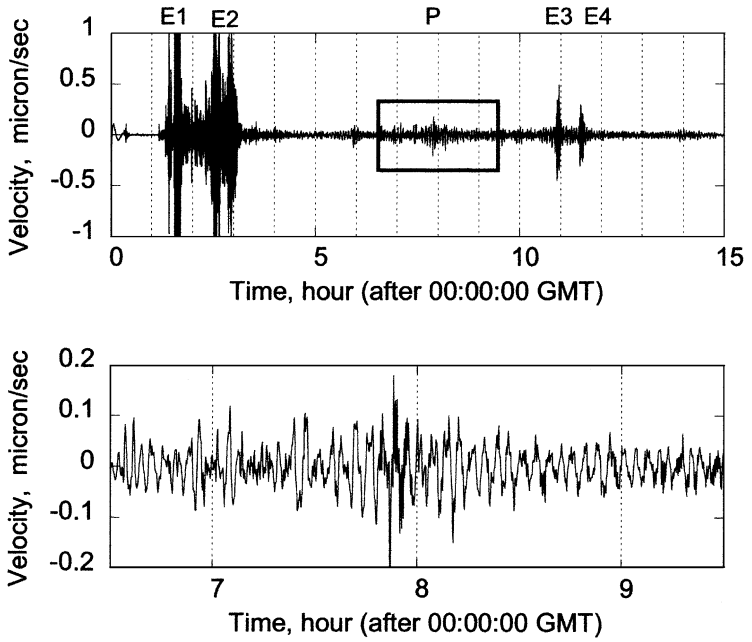

Fig. 2. Top: The vertical component seismogram of the 1991 Pinatubo eruption recorded at Matsushiro, Japan ($\Delta = 26.4°$). The ground-motion velocity is shown. "P" indicates the nearly harmonic oscillation with a period of approximately 230 s excited by the Pinatubo eruption. "E1" and "E2" indicate earthquakes in the Caucasus ($M = 6.3$) and the South Sandwich Islands ($M = 6.5$), respectively. These earthquakes are coincidental and not related to the eruption. "E3" and "E4" indicate two earthquakes ($M = 5.5$ and 5.3, respectively) in the Philippines associated with the eruption. Bottom: Enlarged record of the section in the box shown in the top figure.

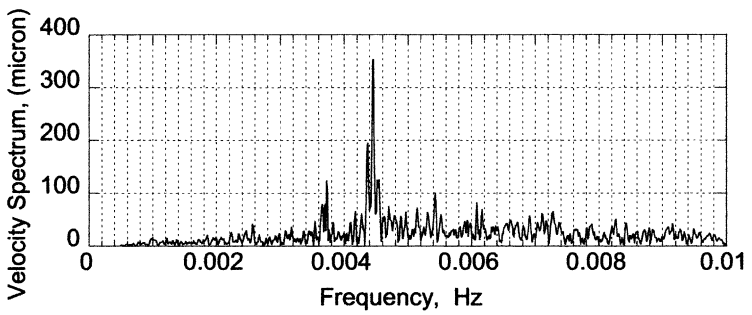

Fig. 3. The spectrum of the nearly harmonic oscillation excited by the Pinatubo eruption showing two peaks at 0.0044 Hz (228 s) and 0.0037 Hz (270 s).

show, using (9) to (11), that if the atmosphere is excited by a horizontal planar source $p_s \exp[i\omega t]$ at $z = 0$, then

$$w = \frac{i\omega c}{2\gamma(\omega_a^2 - \omega^2)^{1/2}}[p_s/p_0(0)]\exp\left\{\left[\frac{\omega_a}{c} \mp \frac{1}{c}(\omega_a^2 - \omega^2)^{1/2}\right] z\right\} \exp[i\omega t] \tag{14}$$

and a resonance occurs at $\omega = \omega_a$.

This result supports the conclusion that the dominant peak observed for the Pinatubo eruption corresponds to this oscillation with the acoustic cut-off frequency.

2.4. Point source

The situation for a point source is somewhat different. Because the wave energy propagates away horizontally, the above resonance does not occur.

The point source problem has been discussed by Weston (1961a, b), Row (1967), Pierce (1963), Ben-Menahem and Singh (1981) and Harkrider (unpublished note). One of the simplest cases is for a "mass injection" point source which is represented by a source term

$$4\pi F_{\mathrm{M}} \exp[\mathrm{i}\omega t]\delta(\bar{R} - \bar{R}_{\mathrm{s}}) \tag{15}$$

to be added to the right-hand side of (7) for mass conservation. Here $\bar{R}$ is the position vector and $\bar{R}_{\mathrm{s}} = (0, 0, z_{\mathrm{s}})$ is the location of the point source, and F_{M} is the mass injected per unit time. The solution for this problem is given by Ben-Menahem and Singh (1981) and Harkrider (unpublished note) as

$$p(r,z,t) = \mathrm{i}\omega F_{\mathrm{M}} \exp\left(-\frac{z-z_{\mathrm{s}}}{2H}\right) \frac{(\omega^2-\omega_{\mathrm{b}}^2)^{1/2}}{(\omega^2-\omega_{\mathrm{c}}^2)^{1/2}} \frac{1}{R} \exp\left[\mathrm{i}\omega\left(t \pm \frac{R}{C}\right)\right], \tag{16}$$

where

$$R^2 = r^2 + (z-z_{\mathrm{s}})^2, \quad r^2 = x^2 + y^2, \quad \omega_{\mathrm{c}} = \frac{|z-z_{\mathrm{s}}|}{R}\,\omega_{\mathrm{b}},$$

and

$$C = \frac{c\omega(\omega^2-\omega_{\mathrm{b}}^2)^{1/2}}{(\omega^2-\omega_{\mathrm{c}}^2)^{1/2}(\omega^2-\omega_{\mathrm{a}}^2)^{1/2}}. \tag{17}$$

The plus or minus sign in (16) should be chosen to satisfy the radiation and causality conditions. For an observer at $r = 0$, $\omega_{\mathrm{c}} = \omega_{\mathrm{b}}$ and we obtain from (16) that

$$p(0,z,t) = \mathrm{i}\omega F_{\mathrm{M}} \exp\left(-\frac{z-z_{\mathrm{s}}}{2H}\right) \frac{1}{R} \exp\left[\mathrm{i}\omega\left(t \pm \frac{R}{C}\right)\right], \tag{18}$$

where

$$C = \frac{c\omega}{(\omega^2-\omega_{\mathrm{a}}^2)^{1/2}}. \tag{19}$$

For a mass injection source which varies as a step function, the pressure change can be computed by integrating (18) with ω. When $r = 0$, the integral can be obtained in a closed form as (Row, 1967)

$$\begin{aligned} p_{\mathrm{H}}(0,z,t) &= \frac{1}{2\pi|z-z_{\mathrm{s}}|} F_{\mathrm{M}} \exp\left[-\frac{z-z_{\mathrm{s}}}{2H}\right] \int_{-\infty}^{+\infty} \exp\{\mathrm{i}[\omega t \pm t_0(\omega^2-\omega_{\mathrm{a}}^2)^{1/2}]\}\,\mathrm{d}\omega \\ &= \frac{1}{|z-z_{\mathrm{s}}|} F_{\mathrm{M}} \exp\left[-\frac{z-z_{\mathrm{s}}}{2H}\right] \left\{\delta(t-t_0) - \frac{\omega_{\mathrm{a}} t_0 J_1[\omega_{\mathrm{a}}(t^2-t_0^2)^{1/2}]}{(t^2-t_0^2)^{1/2}} H(t-t_0)\right\}. \end{aligned} \tag{20}$$

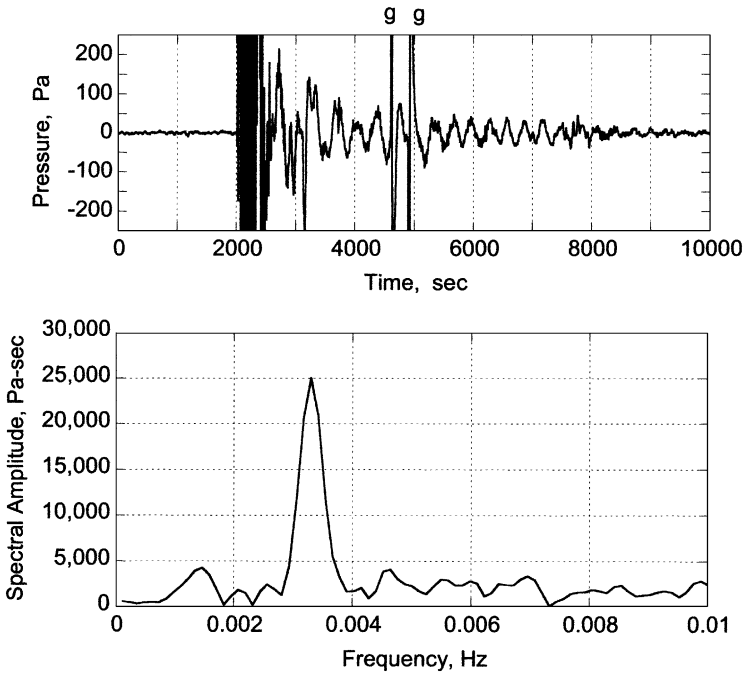

Fig. 4. The atmospheric gravity-mode oscillation excited by the 1980 Mount St. Helens eruption, and was recorded at station LON (Longmire, Washington) at a distance of 67 km. The two spikes at about 5000 s are instrumental glitches. Bottom: Spectrum of the record shown above. The spectrum is computed for the record section after the glitches.

The first term in the bracket (delta function) represents the direct effect. The second term represents atmospheric oscillations. Since

$$J_1(\xi) \propto \sqrt{\frac{2}{\pi\xi}} \cos\left(\xi - \frac{3}{4}\pi\right)$$

for large ξ, the second term represents an oscillation with the angular frequency ω_a, the acoustic cut-off frequency, at large t. Eq. (20) provides the basic mechanism of the atmospheric acoustic waves excited by the 1991 Pinatubo eruption.

More recently, attempts were made to apply the normal-mode theory to the solid-ocean-atmosphere coupled system to investigate this problem more quantitatively (Watada, 1995; Lognonne et al., 1998). Watada (1995) and Lognonne et al. (1998) showed that the oscillation with a period of 270 s is a fundamental mode of Earth's atmosphere and that with a period of 228 s is the first overtone. These periods are close to those of two modes of the solid Earth and the atmospheric modes couple efficiently to the solid Earth modes.

In contrast to the acoustic waves, gravity waves do not couple to the ground efficiently because of the mismatch of the wavelength. Thus, these modes cannot be observed with seismographs and can be recorded only with barographs. For the 1980 Mount St. Helens eruption, gravity-mode atmospheric oscillations with a period of about 300 s were observed with a barograph near the volcano (Kanamori et al., 1994), as shown in Fig. 4.

A simple model for excitation of gravity waves can be obtained by using a point energy injection source given by

$$4\pi F_{\mathrm{E}} \exp[\mathrm{i}\omega t]\delta(\bar{R} - \bar{R}_{\mathrm{s}}), \tag{21}$$

which is added to the right-hand side of the energy equation (8).

The solution is more complicated than that for the mass injection source, but the pressure perturbation at $z = z_{\mathrm{s}}$ is given by

$$p_{\mathrm{H}}(r,z,t) = \frac{F_{\mathrm{E}}}{2\pi c^2 R} \int_{-\infty}^{+\infty} \frac{\omega}{(\omega^2 - \omega_{\mathrm{b}}^2)^{1/2}} \left(1 - \frac{g}{2\omega^2 H}\right) \exp\left[\mathrm{i}\omega\left(t \pm \frac{R}{C}\right)\right] \mathrm{d}\omega. \tag{22}$$

Because of the term $1/(\omega^2 - \omega_{\mathrm{b}}^2)^{1/2}$ in the integrand, this yields gravity waves, and we believe that (22) provides the basic mechanism of the atmospheric oscillations excited by the 1980 Mount St. Helens eruption.

At present, only simple models have been used for the source and the atmospheric structure, and only an order of magnitude energy estimate has been obtained. In particular, it is not clear how to represent the eruption process in the source term. In the simple model we discussed above, we add a source term in the mass or energy equation. It would be equally possible to include the source in the momentum equation as a pressure source. These questions have not been addressed yet, but as the method improves, it will be possible to assess the total thermal energy more accurately, and also to determine the vertical distribution of the thermal energy emitted by the eruption. This method would be useful for a better assessment of the global volcanic hazard immediately after a very large eruption. It is especially important because many active volcanoes are not easily accessible by field observations, and remote sensing using barographs and seismographs is often the only means for assessing the impact of a large eruption.

3. Waves from Shoemaker-Levy 9 comet impacts in Jupiter's atmosphere

The impact of a large comet, Shoemaker-Levy 9, in Jupiter's atmosphere in 1994 produced a ring-like pattern in Jupiter's atmosphere as shown in Fig. 5 (left). Although the cause of this ring-like pattern is not fully understood, the ring appeared to have propagated outward at a speed of 450 m/s, as shown by the time-distance curve (Fig. 6) which was constructed from the several images taken for the impacts of different fragments of the comet. Ingersoll et al. (1994), Ingersoll and Kanamori (1995a, b) interpreted this as a long gravity wave trapped in a wave-guide in Jupiter's atmosphere i.e., waves in the lower-right stippled region in Fig. 1b, where the angular frequency, ω, is lower than the Brunt-Väisälä frequency, $N(=\omega_{\mathrm{b}})$.

3.1. Method

Here, we briefly describe the method used in Ingersoll et al. (1994). The basic equations are similar to those given by (6) to (8). An energy source

$$\gamma\rho_0\kappa\dot{Q}, \tag{23}$$

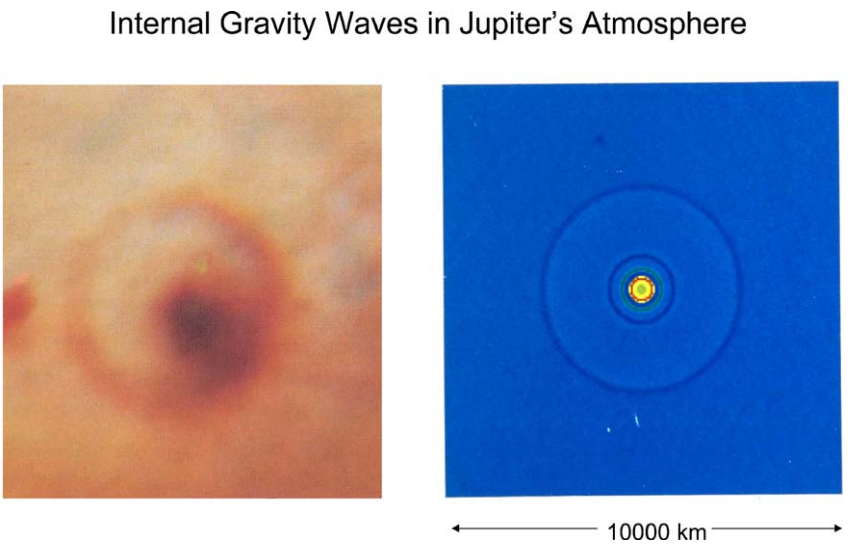

Fig. 5. Left: Hubble Space Telescope image of the impact site of the G fragment of the Shoemaker-Levy 9 comet. The image was taken at 109 min after the impact. The radius of the prominent dark ring is 3700 km (from the cover page of Nature, 374, No. 6524, 1995). Right: Synthetic ring pattern computed for the 10 × solar case. Note the approximate agreement of the positions of the outer and inner rings between the observed and synthetic patterns.

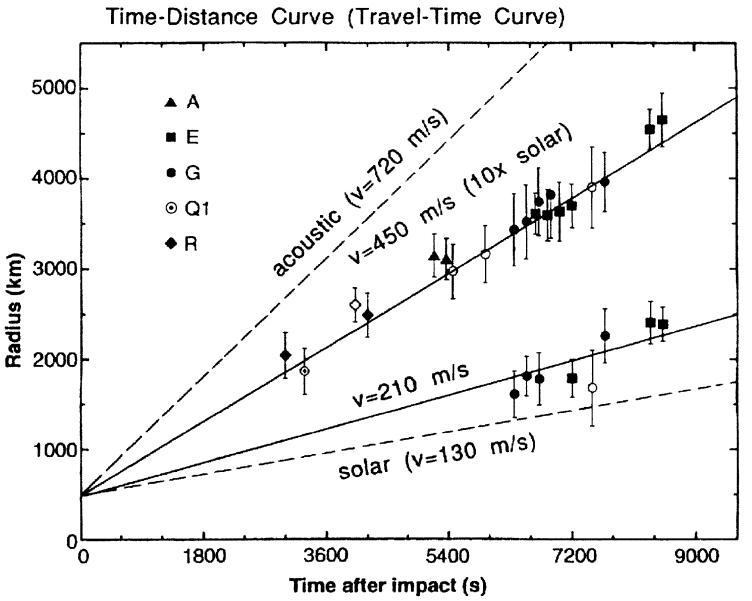

Fig. 6. Time–distance curve for the circular rings shown in Fig. 5. The shape of the symbols identifies the fragments A, E, G, Q1, and R. "Acoustic" refers to the speed of sound at the temperature minimum in Jupiter's atmosphere. "solar" and "10 × solar" refer to the speed of a gravity wave in the water cloud with solar and 10 × solar abundance of water. The data points around the line with $v = 210$ m/s are for the inner rings. Redrawn from Hammel et al. (1995), and Ingersoll and Kanamori (1995b).

where $\dot{Q}$ is the heat source ($\kappa = 1 - 1/\gamma$) is included in the right-hand side of the energy equation (8). Rewriting these equations in the cylindrical coordinate system (r, θ, ϕ) with the assumption of the hydrostatic condition (i.e., long-wave approximation) and the inclusion of the rotation effect, we obtain,

$$\frac{\partial u}{\partial t} - fv = -\frac{1}{\rho_0}\frac{\partial p}{\partial r}, \quad \frac{\partial v}{\partial t} + fu = 0, \quad \frac{\partial p}{\partial z} = -\rho g, \tag{24}$$

$$\frac{\partial p}{\partial t} + w\frac{\partial \rho_0}{\partial z} + \rho_0\left(\frac{1}{r}\frac{\partial (ru)}{\partial r} + \frac{\partial w}{\partial z}\right) = 0, \tag{25}$$

$$\frac{\mathrm{d}p}{\mathrm{d}t} = c^2\frac{\mathrm{d}\rho}{\mathrm{d}t} + \gamma\kappa\rho_0\dot{Q}, \tag{26}$$

where (u, v) denotes (u_r, u_θ), and f is the local Coriolis parameter (i.e., f-plane approximation). We then further rewrite these equations in the isobaric coordinate system with $(u, v, \omega, \Phi, \alpha)$ as dependent variables, where $\Phi = gz$ is the geopotential,

$\omega = (\mathrm{d}p/\mathrm{d}t)$ is the vertical velocity, $\alpha = (1/\rho)$ and

$$\sigma = -\left(\frac{\mathrm{d}\alpha}{\mathrm{d}p} + \frac{\alpha}{\gamma p}\right). \tag{27}$$

The resulting equations are

$$\frac{\partial u}{\partial t} - fv = -\frac{\partial \Phi}{\partial r}, \quad \frac{\partial v}{\partial t} + fu = 0, \quad \frac{\partial \Phi}{\partial p} + \alpha = 0, \tag{28}$$

$$\frac{1}{r}\frac{\partial (ru)}{\partial r} + \frac{\partial \omega}{\partial p} = 0, \tag{29}$$

$$\frac{\partial \alpha}{\partial t} - \sigma\omega = \frac{\kappa\dot{Q}}{p}. \tag{30}$$

Eliminating u, v, ω, and α from (28) to (30), we obtain an equation for Φ as

$$\frac{\partial}{\partial t}\left[\left(\frac{\partial^2}{\partial t^2} + f^2\right)\frac{\partial}{\partial p}\left(\frac{1}{\sigma}\frac{\partial \Phi}{\partial p}\right) + \frac{1}{r}\frac{\partial}{\partial r}\left(r\frac{\partial \Phi}{\partial r}\right)\right] = -\left(\frac{\partial^2}{\partial t^2} + f^2\right)\frac{\partial}{\partial p}\left(\frac{\kappa\dot{Q}}{\sigma p}\right). \tag{31}$$

Ingersoll and Kanamori (1995a) solved this equation for Φ almost analytically, using σ which is derived from the approximate temperature profile in Jupiter's atmosphere shown in Fig. 7.

The heat source caused by the comet impact is given by

$$\dot{Q}(p, r, t) = \eta(p)\delta(r)\delta(t), \tag{32}$$

where a line heating source and delta functions for t and r are used. Then, the following separation of variables,

$$\Phi(p, r, t) = \phi(p)\Gamma(r, t) \tag{33}$$

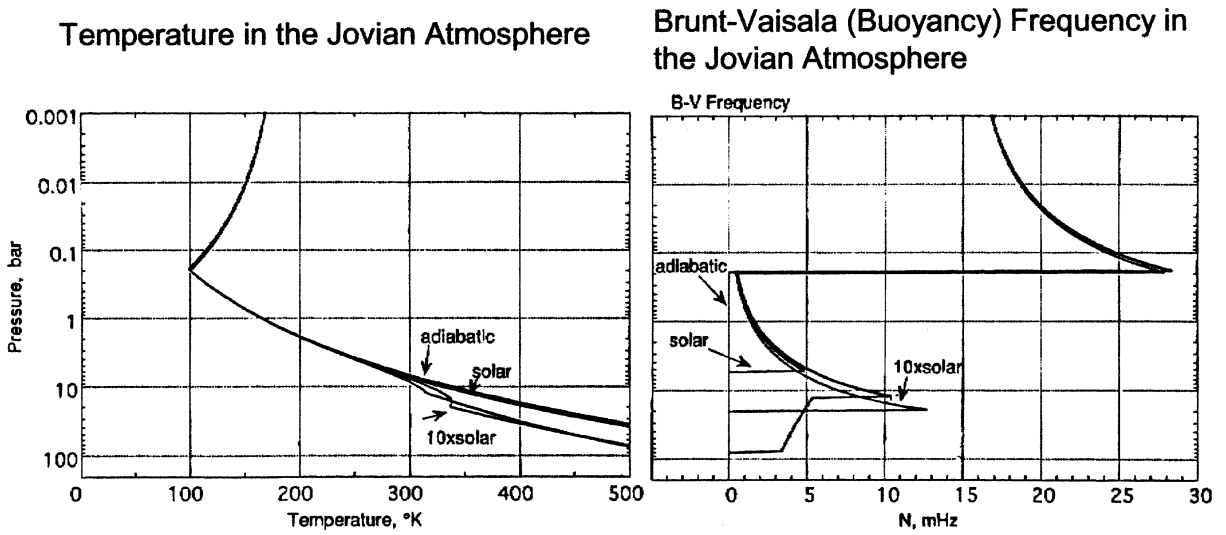

Fig. 7. Left: Temperature profiles for the no-water (adiabatic), solar, 5 × solar (not labeled), and 10 × solar cases used by Ingersoll and Kanamori (1995a). Right: The profiles of the Brunt-Väisälä frequency corresponding to the temperature profiles shown on the left.

leads to

$$\frac{\partial}{\partial t}\left[\left(\frac{\partial^2 \Gamma}{\partial t^2}+f^2\Gamma\right)\frac{\mathrm{d}}{\mathrm{d}p}\left(\frac{1}{\sigma}\frac{\mathrm{d}\phi}{\mathrm{d}p}\right)+\frac{1}{r}\frac{\partial}{\partial r}\left(r\frac{\partial \Gamma}{\partial r}\right)\phi\right]$$
$$=-\left(\frac{\partial^2 \delta(t)}{\partial t^2}+f^2\delta(t)\right)\frac{\mathrm{d}}{\mathrm{d}p}\left(\frac{\kappa\eta(p)}{\sigma p}\right)\delta(r). \tag{34}$$

Then, the vertical normal mode $\phi(p)$ satisfies

$$\frac{\mathrm{d}}{\mathrm{d}p}\left(\frac{1}{\sigma}\frac{\mathrm{d}\phi}{\mathrm{d}p}\right)=-\frac{1}{c^2}\phi(p), \tag{35}$$

where c^2 is the separation constant (unit of velocity).

Let c_i and $\phi_i(p)$ be the ith eigen-value and eigen-function and we expand the heating source, using $\phi_i(p)$, as

$$\frac{\mathrm{d}}{\mathrm{d}p}\left(\frac{\kappa\eta(p)}{\sigma p}\right)=\sum_{i=0}^{\infty}a_i\phi_i(p), \tag{36}$$

where

$$a_i=\frac{\int \frac{\mathrm{d}}{\mathrm{d}p}\left(\frac{\kappa\eta(p)}{\sigma p}\right)\phi_i(p)\,\mathrm{d}p}{\int \phi_i^2(p)\,\mathrm{d}p}. \tag{37}$$

If the rotation effect is ignored, i.e., $f^2 = 0$, then, it follows from (34) that

$$\frac{1}{c_i^2}\frac{\partial^2 \Gamma}{\partial t^2} = \frac{1}{r}\frac{\partial}{\partial r}\left(r\frac{\partial \Gamma}{\partial r}\right) + a_i \delta(r)\dot{\delta}(t). \tag{38}$$

Solution of (38) is given by

$$\Gamma_i(r,t) = \begin{cases} \dfrac{c_i a_i}{2\pi}\dfrac{\partial}{\partial t}\left[\dfrac{1}{\sqrt{c_i^2 t^2 - r^2}}\right] & \text{for } c_i t > r, \\ 0 & \text{for } c_i t \leqslant r. \end{cases} \tag{39}$$

Then, the final solution for $\Phi(p,r,t)$ is given by

$$\Phi(p,r,t) = \sum_{i=0}^{\infty} \frac{a_i c_i}{2\pi}\phi_i(p)\frac{\partial}{\partial t}\left[\frac{1}{\sqrt{c_i^2 t^2 - r^2}}\right] \quad \text{for } c_i t > r. \tag{40}$$

Then, the temperature perturbation T' is given by

$$T' = -\frac{p}{R}\frac{\partial \Phi}{\partial p}. \tag{41}$$

If the assumption $f^2 = 0$ is removed, the solution of the wave equation corresponding to (38) cannot be obtained by a simple expression given by (39), and the wave equation must be integrated numerically.

3.2. Model and result

A key parameter is the Brunt-Väisälä frequency, N, which is the maximum frequency of a displaced parcel oscillating under its own buoyancy, and determines the velocity of propagation of gravity waves in the wave guide. N^2 is proportional to the difference between the lapse rate of temperature and the adiabatic lapse rate. The vertical distribution of N^2 is determined by the temperature distribution in the wave-guide which is controlled by the water content in the atmosphere through moist convection. Fig. 7 shows the temperature profiles used by Ingersoll and Kanamori (1995a) and the corresponding profiles of the Brunt-Väisälä frequency. A key parameter is e_{H_2O}, the enhancement factor of water relative to the solar abundance, that is, Jupiter's O/H ratio relative to that on the Sun. (Since water is the main oxygen-bearing molecule, the O/H ratio sets the water abundance.) As e_{H_2O} increases, N in the wave-guide increases (i.e., the wave-guide becomes more stable), and the speed of the internal gravity wave increases. Ingersoll and Kanamori (1995a) computed the temperature perturbations excited by an impact for various cases of heating and water content and showed that if the water content of Jupiter's atmosphere is the same as the solar atmosphere (i.e., $e_{H_2O} = 1$) then the propagation speed is 130 m/s. The much faster observed propagation speed of 450 m/s would require $e_{H_2O} = 10$. In moist convection, the higher the water content, the larger is the deviation of the temperature gradient from the dry adiabat. As a result, the waveguide becomes more stable with a higher N and higher propagation speed. Thus, to increase the propagation speed, an increase in e_{H_2O} is required. Fig. 5 compares the ring-like wave front structure computed with $e_{H_2O} = 10$ (right) with the observed image (left). The rings near the center are due to overtones of the gravity waves. Note that the observed image also shows, though faintly, another ring-like structure near the center.

From this comparison, Ingersoll and Kanamori (1995a) concluded that the water content in Jupiter's atmosphere at the comet impact site is approximately 10 times larger than that for the sun.

The later observation by a Galileo probe in December, 1995, however, indicated that Jupiter's atmosphere is dry at least near the landing site of the probe. It turned out that the probe's entry site was unusual. Earth-based observations and more recent observations by the Galileo orbiter showed that the probe entry site is probably one of the warmest and driest areas on Jupiter (e.g., Orton et al., 1998). Jupiter's atmosphere is spatially heterogeneous, and the water content could be different between the impact site of Shoemaker-Levy 9 and the Galileo probe entry site.

Given the limited amount of information, the interpretation of the ring-like structure is not unique and other models are possible. For example, Walterscheid et al. (2000) proposed a model which does not require a stable, water-rich, wave-guide in Jupiter's atmosphere. Walterscheid et al. (2000) performed a finite difference computation for a nonlinear, compressible, cylindrical, axi-symmetric, f-plane model and suggested that the observed ring disturbances are horizontally propagating stratospheric gravity waves. In their model, the waves are excited not by the initial cometary impact, but by the heating of the atmosphere due to the fallback of plume material from the impact. The advantage of Walterscheid et al.'s (2000) model is that it does not require a somewhat extreme atmospheric structure with $e_{H_2O} = 10$. In contrast, Ingersoll and Kanamori's (1995a) model produces a more distinct ring-like pattern which can be directly compared with the observation, as illustrated in Fig. 5. In view of the present uncertainties in the structure of Jupiter's atmosphere, and its lateral variations, both should be regarded as viable models at present.

4. Morning Glory wave

Gossard and Munk (1954) reported observations of atmospheric waves with periods of 5–15 min near San Diego. The propagation speed is about 10 m/s. They interpreted these waves as internal gravity waves trapped in a wave guide formed by a temperature inversion over the area (i.e., waves in the lower-right stippled region in Fig. 1b).

For many years, people living near the Gulf of Carpentaria in Australia have observed spectacular roll clouds. Due to their frequent morning occurrences, natives dubbed the strange atmospheric phenomenon the "morning glory". Christie et al. (1978) made an extensive study on this using seismographic and barographic observations, and concluded that the morning glory is caused by an internal, non-linear gravity wave in the atmosphere.

We have recently observed in southern California, with broad-band seismometers and barographs, atmospheric disturbances with a period of about 1000 s and pressure amplitude of about 0.5 mbar (Fig. 8). This wave travels at a speed of about 10 m/s across the Los Angeles basin (Fig. 9). A preliminary investigation (Tsai et al., 2003) suggests that this wave is similar to those observed by Gossard and Munk (1954) near San Diego, and the Morning Glory wave observed in Australia (Christie, 1992). It was probably excited in a wave-guide (about 1 km thick) which is formed by temperature inversion in the Los Angeles basin by a rapid downdraft caused by the Santa Ana type condition or by a storm coming into the Los Angeles basin.

When the condition for temperature inversion prevails, the perturbation ΔT from the normal temperature is usually about 1% of the background temperature, T, (i.e., $\Delta T/T = 0.01$) and the corresponding relative density perturbation, $\Delta\rho/\rho$, is about 0.01. Hence, if a simple two-layered

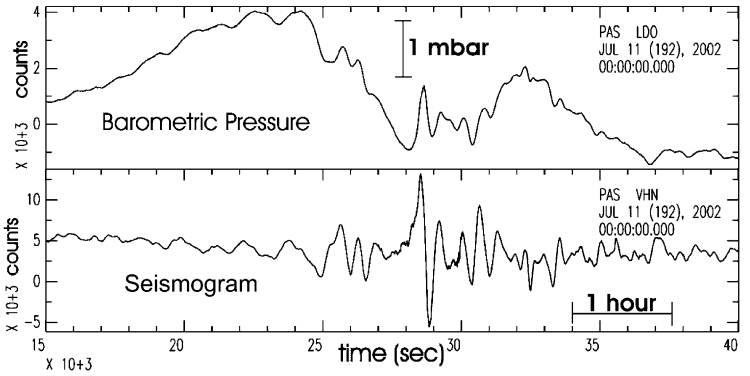

Fig. 8. A slow atmospheric wave observed in the Los Angeles basin. The top figure shows the pressure change and the bottom figure shows the corresponding seismogram.

(i.e., a half-space over a layer with a thickness of h) model is used, the pressure change, Δp, is approximately given by $\Delta p = ga\Delta\rho$ where a is the undulation of the boundary and g is the acceleration of gravity. Then, with $\Delta\rho = 0.01 \times \rho = 1.293 \times 10^{-5}$ g/cm^3, the observed large (0.5 mbar) pressure perturbation suggests $a \approx 395$ m, a substantial fraction of the layer thickness, $h \approx 1$ km. Thus, it is likely that the wave which is initially formed as a linear internal gravity wave, as discussed by Gossard and Munk (1954), later develops to a non-linear wave. If it is fully developed to a non-linear solitary wave, as discussed by Christie et al. (1978), the velocity is given by (Benjamin, 1967)

$$c = (gh\Delta\rho/\rho)^{1/2}(1 + 3a/4h)^{1/2},$$

and the effective pulse width τ is given by

$$\tau = (16/3)(h^2/ac).$$

Substituting the values of a, g, h, and $\Delta\rho$ in these relations, we obtain $c = 11.3$ m/s and $\tau = 1200$ s, which are in approximate agreement with the observed speed and the period.

These results suggest that the slow atmospheric waves observed in the Los Angeles basin are similar to those studied by Gossard and Munk (1954) and Christie et al. (1978). The waves observed in the Los Angeles basin are sometimes pulse-like (e.g., Fig. 8), and sometimes dispersive wave trains (Fig. 9), which suggests that they are not always fully developed non-linear solitary waves.

Although the geophysical implication of these results is not clear yet, with the dense seismographic and barographic network in southern California and Japan, this finding will attract geophysicists' interest in the interaction between the atmosphere and the solid earth.

5. Elasto-hydrodynamic lubrication during earthquake faulting

Sommerfeld (see p. 253 of Sommerfeld, 1950) developed a theory of mechanical lubrication for a journal-bearing system (Fig. 10). Brodsky and Kanamori (2001) applied the theory to earthquake faulting. In a journal-bearing system, two length scales, L (circumference of the journal) and the

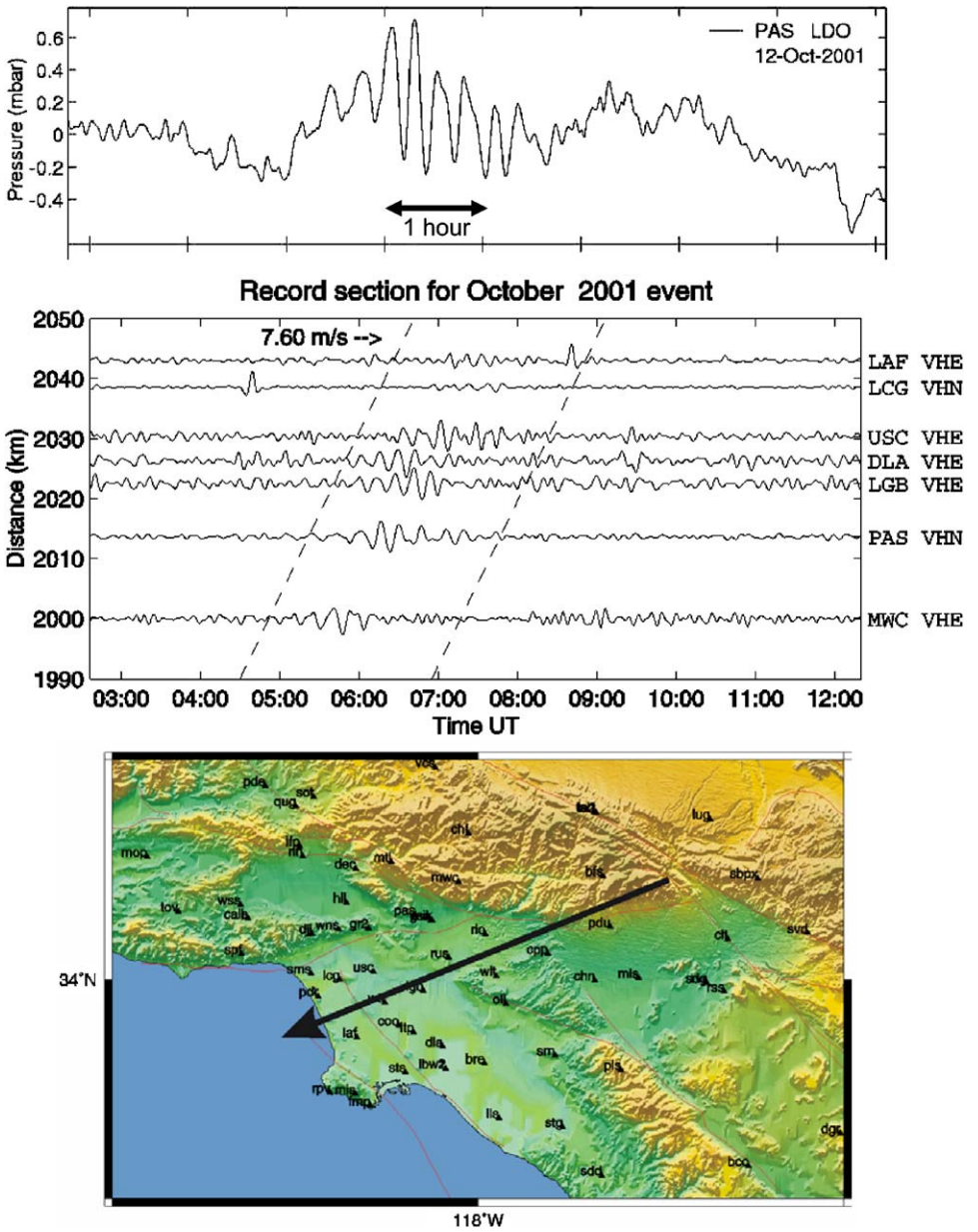

Fig. 9. Top: A barograph record. Middle: A seismogram record section showing the propagation of the atmospheric wave across the Los Angeles basin. Bottom: Distribution of the recording stations and the approximate propagation path.

gap d, and the viscosity of fluid, η, play a key role in lubrication. If a seismic fault zone is thin and rough, and if the material in the fault zone behaves like a viscous fluid, then this theory can be applied to seismic faulting (Fig. 11). In this case, d is the thickness of the slip zone, L is proportional to the amount of fault displacement (i.e., the horizontal length scale evolves as the fault

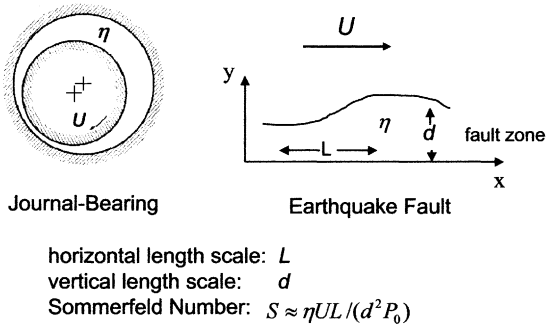

Fig. 10. A journal-bearing system described in Sommerfeld (1954) (left) and its application to earthquake faulting (right). The horizontal length scale L, the vertical length scale, d, the viscosity η, and the speed of the motion, U, control hydrodynamic lubrication. The non-dimension parameter, S (Sommerfeld number), determines the mode of lubrication.

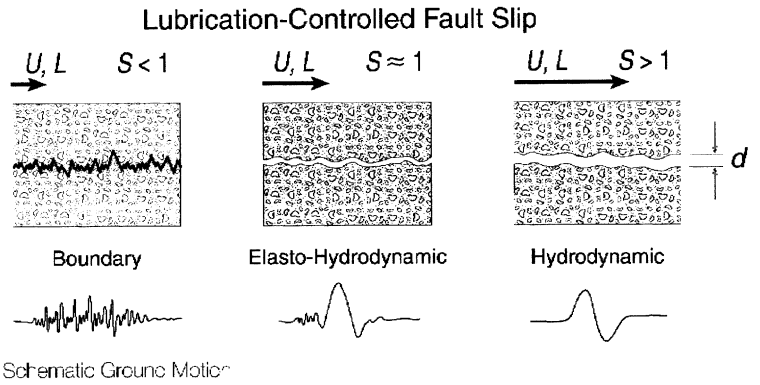

Fig. 11. Schematic figure showing the difference in lubrication as S increases. Left: When S is small, hydrodynamic lubrication is not effective, and boundary lubrication dominates. As a result, high-frequency waves are excited due to collision of small scale heterogeneities (asperities) on the fault walls. Middle: When $S \approx 1$, hydrodynamic lubrication takes effect. As a result, kinetic friction decreases and the speed of fault motion increases. The wall is flattened by elastic deformation and the gap is widened because of increased lubrication pressure. Excitation of high-frequency energy due to collision of asperities is then suppressed. Right: As S further increases, hydrodynamic lubrication dominates. Ground motions resulting from fault motion are shown schematically at the bottom.

slip increases, see Brodsky and Kanamori, 2001), and U is the ground-motion velocity. The thin gap simplification of the Navier–Stokes equation is known as the lubrication equation in which the terms of the order of $(d/L)^2$ or smaller are neglected, and the Raynolds number is assumed to be much smaller than (L/d). During seismic faulting, both conditions are met and the governing equations in two dimensions are

$$\frac{\partial p}{\partial x} = \eta \frac{\partial^2 u}{\partial z^2} \quad \text{and} \quad \frac{\partial p}{\partial z} = 0,$$

where u is the fluid velocity, p is the pressure, and η is the viscosity, and x is taken in the direction of fault strike and z is taken normal to it.

A dimensionless number $S=(P_L/P_0)=6\eta UL/(d^2P_0)$ (U = speed, P_0 = ambient pressure), called the Sommerfeld number, is the ratio of lubrication pressure, $P_L = 6\eta UL/d^2$, to the ambient pressure, P_0, and determines the mode of lubrication. As schematically illustrated in Fig. 11, as the displacement and velocity of fault motion increase, S increases and the lubrication pressure within the fault zone rises. The increased lubrication pressure reduces friction and increases the velocity of fault motion which is driven by the tectonic stress (the velocity of fault motion is proportional to the tectonic stress minus friction); the lubrication pressure also elastically deforms the fault wall, widens the gap, and reduces the contact area between the asperities (rough spots) on the fault walls. This results in reduction in high-frequency energy radiation produced by asperity collisions (Fig. 11, middle). During the recent Chi-Chi, Taiwan, earthquake (September 20, 1999, $M_W = 7.6$), the observed ground-motion velocity near the northern end of the fault was extremely large (about 3 m/s, the largest ever recorded), but short period acceleration was not particularly strong so that the damage to ordinary structures by shaking was minor (Fig. 12). This counter-intuitive observation could be a manifestation of the lubrication effects (Ma et al., 2003), as illustrated in Fig. 12. The difficulty in applying this model to seismic faulting is that very little is known about some of the key parameters. For example, we do not know the thickness of the fault zone, d, very well, and how the horizontal length scale, L, evolves with fault slip is not known. Also, the viscosity of the material in the fault zone is uncertain, and it may depend drastically on the temperature in the fault zone. Thus, it is difficult to prove that this mechanism is indeed working during an earthquake. However, the Sommerfeld number, S, estimated for a reasonable range of parameters, can have a value close to 1 for large earthquakes with $M > 6$, which suggests that this lubrication mechanism can be important for large earthquake.

The elasto-hydrodynamic lubrication is not the only mechanism and other lubrication mechanisms are also possible. For example, if fluid exists in a fault zone it will work as lubricant when heated (i.e., fluid pressurization, Sibson, 1973). If a fault zone is dry, shear heating during faulting may cause melting and lubrication (Jeffreys, 1942). The actual fault motion may involve all of these mechanisms depending on the physical condition in the fault zone.

Since long-period ground motion with a large slip velocity has an important influence on large structures such as high-rise buildings and bridges, this result may have an important engineering implication. However, since this is the only earthquake for which such large slip and slip velocity were instrumentally observed, whether this is indeed a general behavior or not is yet to be seen.

6. Conclusion

This paper illustrates a few examples in which very simple fluid mechanical models can be used to understand the basic physics behind some initially mysterious observations in geophysics. Although the real processes must involve far more complex mechanisms than those included in the simple models illustrated above, we hope that, once the basic physics is understood with simple models, more detailed numerical methods which include all the relevant mechanisms can be developed to fully understand the complex natural processes.

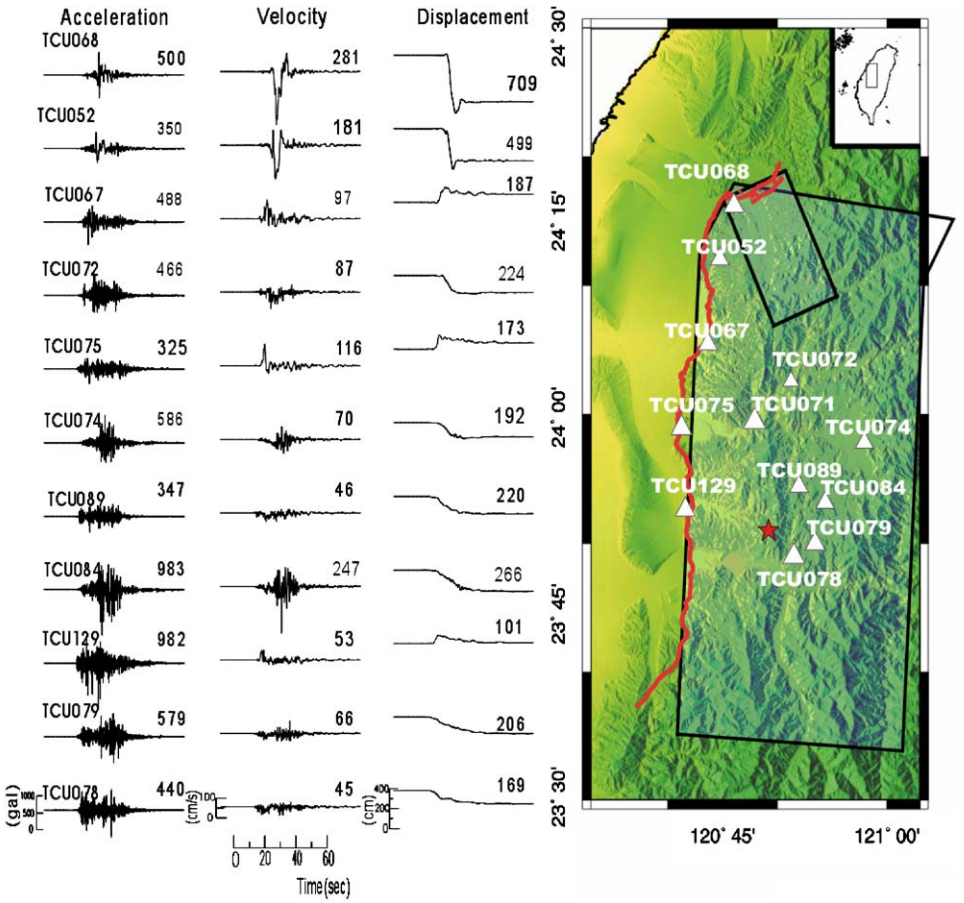

Fig. 12. Ground-motion acceleration, velocity and displacement at stations along the fault of the 1999 Chi-Chi, Taiwan, earthquake ($M_W = 7.6$). The records for stations are arranged from north to south. The number on each seismogram indicates the maximum amplitude in cgs units. The surface breaks of the Chelungpu fault are shown by a bold curve. Note that the stations near the northern end of the fault display large velocity and displacement, but relatively small and short acceleration records. In contrast, the stations to the south display small velocity and displacement, but relatively large acceleration (Ma et al., 2003). Compare this pattern with that shown in Fig. 11.

References

Ben-Menahem, A., Singh, S.J., 1981. Seismic Waves and Sources, Springer, New York, pp. 1–1108.

Benjamin, T.B., 1967. Internal waves of permanent form in fluids of great depth. J. Fluid Mech. 29, 559–592.

Blanc, E., 1985. Observations in the upper atmosphere of infrasonic waves from natural or artificial sources: a summary. Ann. Geophys. 3, 673–688.

Bolt, B.A., Tanimoto, T., 1981. Atmospheric oscillations after the May 18, 1980 eruption of Mount St. Helens. EOS 62, 529.

Brodsky, E.E., Kanamori, H., 2001. The elastohydrodynamic lubrication of faults. J. Geophys. Res. 106, 16,357–16,374.

Christie, D.R., 1992. The morning glory of the Gulf of Carpentaria: a paradigm for non-linear waves in the lower atmosphere. Aust. Meteorol. Mag. 41, 21–60.

Christie, D.R., Muirhead, K.J., Hales, A.L., 1978. On solitary waves in the Atmosphere. J. Atmos. Sci. 35, 805–825.

Gill, A., 1982. Atmosphere-Ocean Dynamics. Academic Press, San Diego, pp. 662.

Gossard, E., Munk, W., 1954. On gravity waves in the atmosphere. J. Meteorol. 11, 259–269.

Hammel, H.B., et al., 1995. HST imaging of atmospheric phenomena created by impact of comet Shoemaker-Levy 9. Science 267, 1288–1296.

Harkrider, D.G., Press, F., 1967. The Krakatoa air-sea waves: an example of pulse propagation in coupled systems. Geophys. J. Astron. Soc. 13, 149–159.

Hines, C.O., 1960. Internal atmospheric gravity waves at ionospheric heights. Can. J. Phys. 38, 1441.

Houghton, J.T., 1986. The Physics of Atmospheres, 2nd Edition. Cambridge University Press, New York, 271pp.

Ingersoll, A.P., Kanamori, H., 1995a. Waves from the collisions of Shoemaker-Levy 9 with Jupiter. Nature 374, 706–708.

Ingersoll, A.P., Kanamori, H., 1995b. Waves from the Shoemaker-Levy 9 impacts. Noll, K.S., Weaver, H.A., Feldman, P.D. (Eds.), Proceedings of the Space Telescope Science Institute Workshop, Baltimore, MD., May 9–12, Cambridge University Press, Cambridge, pp. 329–345.

Ingersoll, A.P., Kanamori, H., Dowling, T.E., 1994. Atmospheric gravity waves from the impact of comet Shoemaker-Levy 9 with Jupiter. Geophys. Res. Lett. 21, 1083–1086.

Jeffreys, H., 1942. On the mechanics of faulting. Geol. Mag. 79, 291–295.

Kanamori, H., Mori, J., 1992. Harmonic excitation of Mantle Rayleigh waves by the 1991 eruption of Mount Pinatubo, Philippines. Geophys. Res. Lett. 19, 721–724.

Kanamori, H., Mori, J., Harkrider, D.G., 1994. Excitation of atmospheric oscillations by volcanic eruptions. J. Geophys. Res. 99, 21,947–21,961.

Lamb, H., 1932. Hydrodynamics, 6th Edition. Dover Publication, New York, pp. 1–738.

Lognonne, P., Clévédé, E., Kanamori, H., 1998. Computation of seismograms and atmospheric oscillations by normal-mode summation for a spherical earth model with realistic atmosphere. Geophys. J. Int. 135, 388–406.

Ma, K.-F., Brodsky, E.E., Mori, J., Ji, C., Song, T-R.A., Kanamori, H., 2003. Evidence for fault lubrication during the 1999 Chi-Chi, Taiwan, Earthquake (Mw7.6). Geophys. Res. Lett. 30 (5), 1244. 48-1:48-4, 10.1029.

Orton, G.S., Fisher, B.M., Baines, K.H., et al., 1998. Characteristics of the Galileo probe entry site from earth-based remote sensing observations. J. Geophys. Res. 103, 22,791–22,814.

Pierce, A.D., 1963. Propagation of acoustic-gravity waves from a small source above the ground in an isothermal atmosphere. J. Acoust. Soc. Am. 35, 1798–1807.

Row, R.V., 1967. Acoustic-gravity waves in the upper atmosphere due to a nuclear detonation and an earthquake. J. Geophys. Res. 72, 1599–1610.

Schubert, G., Turcotte, D.L., Olson, P., 2001. Mantle Convection in the Earth and Planets, Cambridge University Press, Cambridge, 940p.

Sibson, R.H., 1973. Interactions between temperature and fluid pressure during earthquake faulting—a mechanism for partial or total stress relief. Nature 243, 66–68.

Sommerfeld, A., 1950. Mechanics of Deformable Bodies. Academic Press, San Diego.

Tsai, V.C., Kanamori, H., Artru, J., 2003. The Morning-Glory wave of Southern California. J. Geophys. Res., in press.

Walterscheid, R.L., Brinkman, D.G., Schubert, G., 2000. Wave disturbances from the comet SL-9 impacts into Jupiter's atmosphere. ICARUS 145, 140–146.

Watada, S., 1995. Part I: Near-source acoustic coupling between the atmosphere and the solid earth during volcanic eruptions. Part II: Nearfield normal mode amplitude anomalies of the Landers Earthquake. Ph.D. Thesis, California Institute of Technology, Pasadena.

Weston, V.H., 1961a. The pressure pulse produced by a large explosion in the atmosphere. Can. J. Phys. 39, 993–1009.

Weston, V.H., 1961b. The pressure pulse produced by a large explosion in the atmosphere. Part II. Can. J. Phys. 40, 431–445.

Widmer, R., Zürn, W., 1992. Bichromatic excitation of long-period Rayleigh and air waves by the Mount Pinatubo and El Chichón volcanic eruption. Geophys. Res. Lett. 19, 765–768.